Progress in PHOTOVOLTAICS

PROGRESS IN PHOTOVOLTAICS: RESEARCH AND APPLICATIONS
Prog. Photovolt: Res. Appl. 2014; **22:**51–57
Published online 7 February 2013 in Wiley Online Library (wileyonlinelibrary.com). DOI: 10.1002/pip.2324

RESEARCH ARTICLE

$Cu_2ZnSnSe_4$ thin film solar cells produced via co-evaporation and annealing including a $SnSe_2$ capping layer

Alex Redinger[1]*, Marina Mousel[1], Rabie Djemour[1], Levent Gütay[1], Nathalie Valle[2] and Susanne Siebentritt[1]

[1] Université du Luxembourg, Laboratory for Photovoltaics, 41, rue du Brill, L-4422 Belvaux, Luxembourg
[2] Centre de Recherche Public Gabriel Lippmann, 41, rue du Brill, L-4422 Belvaux, Luxembourg

ABSTRACT

$Cu_2ZnSnSe_4$ (CZTSe) thin film solar cells have been produced via co-evaporation followed by a high-temperature annealing. In order to reduce the decomposition of the CZTSe, a $SnSe_2$ capping layer has been evaporated onto the absorber prior to the high-temperature treatment. This eliminates the Sn losses due to SnSe evaporation. A solar cell efficiency of 5.1% could be achieved with this method. Moreover, the device does not suffer from high series resistance, and the dominant recombination pathway is situated in the absorber bulk. Finally, different illumination conditions (white light, red light, and yellow light) reveal a strong loss in fill factor if no carriers are generated in the CdS buffer layer. This effect, known as red-kink effect, has also been observed in the closely related $Cu(In,Ga)Se_2$ thin film solar cells. Copyright © 2013 John Wiley & Sons, Ltd.

KEYWORDS

$Cu_2ZnSnSe_4$; thin films; semiconductors; co-evaporation; solar cell

***Correspondence**

Alex Redinger, Université du Luxembourg, Laboratory for Photovoltaics, 41, rue du Brill, L-4422 Belvaux, Luxembourg.
E-mail: alex.redinger@uni.lu

Received 14 September 2012; Revised 12 October 2012; Accepted 22 October 2012

1. INTRODUCTION

The $Cu_2ZnSnSe_4$ and Cu_2ZnSnS_4 [CZTS(e)] semiconductor compounds are currently being extensively studied as possible absorber layers for thin film solar cells. The CZTS(e) p-type semiconductor compound exhibits a direct bandgap of 1.0–1.5 eV (depending on the S/Se ratio), a large absorption coefficient, and most elements are highly abundant in the Earth's crust, which makes this material highly interesting for solar cells.

The best-performing devices have already reached a power conversion efficiency of 11.1% [1] in the case of a mixed S/Se absorber and 9.15% [2] for a pure selenium absorber. The production routes described in literature including co-evaporation [2], solution-based methods [3,4], and sputtering [5] are manifold.

Most synthesis techniques use a two-stage process where a precursor is first formed at relatively low temperatures followed by a high-temperature treatment [1,3,4,6–8]. The success of this procedure can be traced back to the fundamental physical properties of the CZTSe material. At temperatures higher than 350°C, CZTSe starts to decompose, and Se and SnSe start to evaporate [9]. The decomposition is not only a problem for the selenide-based absorbers but is independent of the S/Se content. Only the onset temperatures change slightly. In order to prevent this decomposition, a number of different routes such as adding SnSe and Se in excess during the final heat treatment [10], introducing excess chalcogen in the precursor layers [6], excess Sn and Se during co-evaporation [2], or fast heating ramps [11] have been introduced recently. In all cases, the production method aims at reducing the decomposition of the CZTSe at high temperatures [10].

In this paper, we present a modified production method that simplifies the growth of the absorber layers because it eliminates the need to control the Se and SnSe partial pressures during the treatment [12]. A $SnSe_2$ capping layer is evaporated on top of the absorber layer prior to the final heat treatment. The capping layer protects the absorber during the transfer from the vacuum chamber to the annealing chamber and acts as a source of SnSe and Se during the final heat treatment.

A promising solar cell efficiency of 5.1% could be achieved with this method. Moreover, the device does not exhibit a large series resistance, and the performance is not limited by interface recombination. This is in contrast to most devices in literature where dominant interface recombination and a large series resistance are detrimental for high-efficiency solar cells [3,7,10,13].

2. EXPERIMENTAL

The CZTSe absorbers in this study are produced in a molecular beam epitaxy system with Cu, Zn, and Sn evaporation sources, and Se is supplied via a valved source. The deposition temperature has been set to 320°C, and all four elements are co-evaporated on a molybdenum-coated soda lime glass substrate. A stoichiometry of Cu/(Zn+Sn) = 0.8 and Zn/Sn = 1.2 has been set, and a film thickness of roughly 1600 nm has been chosen. In the next step, the sample is cooled down to 150°C, and Sn and Se are co-evaporated on the CZTSe absorber. Thereby a roughly 200-nm-thick $SnSe_2$ layer is formed on top of the CZTSe. The sample is transferred into a tube furnace (see reference [8] for details) and annealed at 500°C for 30 min in the presence of 1-mbar H_2/N_2. Moreover, 20-mg Se in the form of powder has been introduced into the hot zone. Upon heating, a part of the capping layer desorbs and forms a high partial pressure of SnSe and Se above the surface, which protects the film. Because the desorption of the SnSe and Se proceeds exclusively from the surface, the underlying CZTSe is confined, and decomposition is eliminated. After the final heat treatment, the absorber is still covered with a certain amount of $SnSe_x$. In order to remove this detrimental secondary phase, the sample has been etched in concentrated HCl (37 vol%) for 10 min at room temperature. This chemical treatment selectively removes the $SnSe_x$ layer, and the etching rate of the CZTSe is much lower (for the etching conditions used in this study, we do not observe any change in thickness during HCl etching of CZTSe).

The samples are characterized with scanning electron microscopy (SEM) equipped with an energy dispersive X-ray (EDX) analyzer and Raman spectroscopy (514.5-nm excitation wavelength) in order to analyze the near-surface region of the absorber layer. Photoluminescence (PL) at room temperature is used to determine the bandgap of the absorber layer in the near-surface region. Depth profiles have been performed via secondary ion mass spectrometry with a Cs^+ ion gun operating at an energy of 3.5 keV. The elements of interest Cu, Sn, Zn, Se, and Mo were measured as MCs^+ clusters in order to limit matrix effects. The area of investigation was limited to 60 microns in diameter.

Solar cells have been processed in the following way. After HCl etching, the samples are etched in KCN for 30 s followed by chemical bath deposition of CdS. Finally, the n-type window layer is sputtered via radio frequency magnetron sputtering from undoped and Al-doped ZnO followed by e-beam evaporation of Ni–Al grids. The solar cells have been characterized with current–voltage (I–V) measurements and quantum efficiency (QE) measurements. The current–voltage measurements have been performed with a halogen lamp that has been adjusted to 100 mW/cm^2. Some samples have also been analyzed in a temperature-dependent current–voltage characterization setup.

3. RESULTS AND DISCUSSION

In Figure 1(a–f), the SEM micrographs and the Raman spectra of the absorber layer after the different processing steps are presented. After vacuum deposition, including the capping layer, the surface is almost entirely covered with $SnSe_2$ [Figure 1(a)]. The Raman modes at 115 and 183 cm^{-1} [Figure 1(b)] are in good agreement with literature [14]. The Raman modes at 250 and 106 cm^{-1} could be due to amorphous Se in the near-surface region [15]. After the heat treatment [Figure 1(c)], the surface changes significantly, and the topview SEM micrographs show a film that is quite smooth but is not completely covering the underlying material. Raman scattering analysis of this sample shows that the material that is left behind in the near-surface region is almost exclusively SnSe with Raman modes at 100, 126, and 149 cm^{-1}. The assignment has been carried out with the help of commercially available SnSe powder. There is no clear signal from the CZTSe visible in the Raman measurements. Only a small contribution of the main CZTSe peak at 195 cm^{-1} could be identified. This is due to the finite penetration depth of the 514-nm laser line in SnSe, which exhibits an absorption coefficient well above 10^5 cm^{-1} [16]. Solar cells produced from these absorbers without removing the SnSe thin film did not result in working devices. Therefore, as described in the previous section, the samples have been etched in concentrated HCl for 10 min in order to remove the remaining SnSe [Figure 1(e,f)]. The Raman modes of the sample after etching can be assigned exclusively to CZTSe modes at 170, 194, 234, 244 cm^{-1} [17]. The origin of the small contribution at 325 cm^{-1} is not clear at present.

Secondary ion mass spectrometry profiles are shown in Figure 1(g). The intensities of the different elements have been normalized to intensities measured in the middle of the absorber layer. The near-surface region shows nearly the same composition as the bulk. The lower intensity of all elements in the near-surface region compared with that in the bulk is most likely due to a combination of roughness and oxidation.

Moreover, the solar cell absorber layers show a Sn increase towards the Mo back contact. In order to confirm a change in composition, a complementary EDX study was carried out on the absorber after mechanical removal of the film from the substrate. The morphology and an EDX mapping of the backside is shown in Figure 1(h,i). A large number of white spots with a size smaller than 1 μm are visible in the SEM micrographs. In Figure 1(i), an EDX mapping is presented. The Sn L-line intensity is almost

DOI: 10.1002/pip

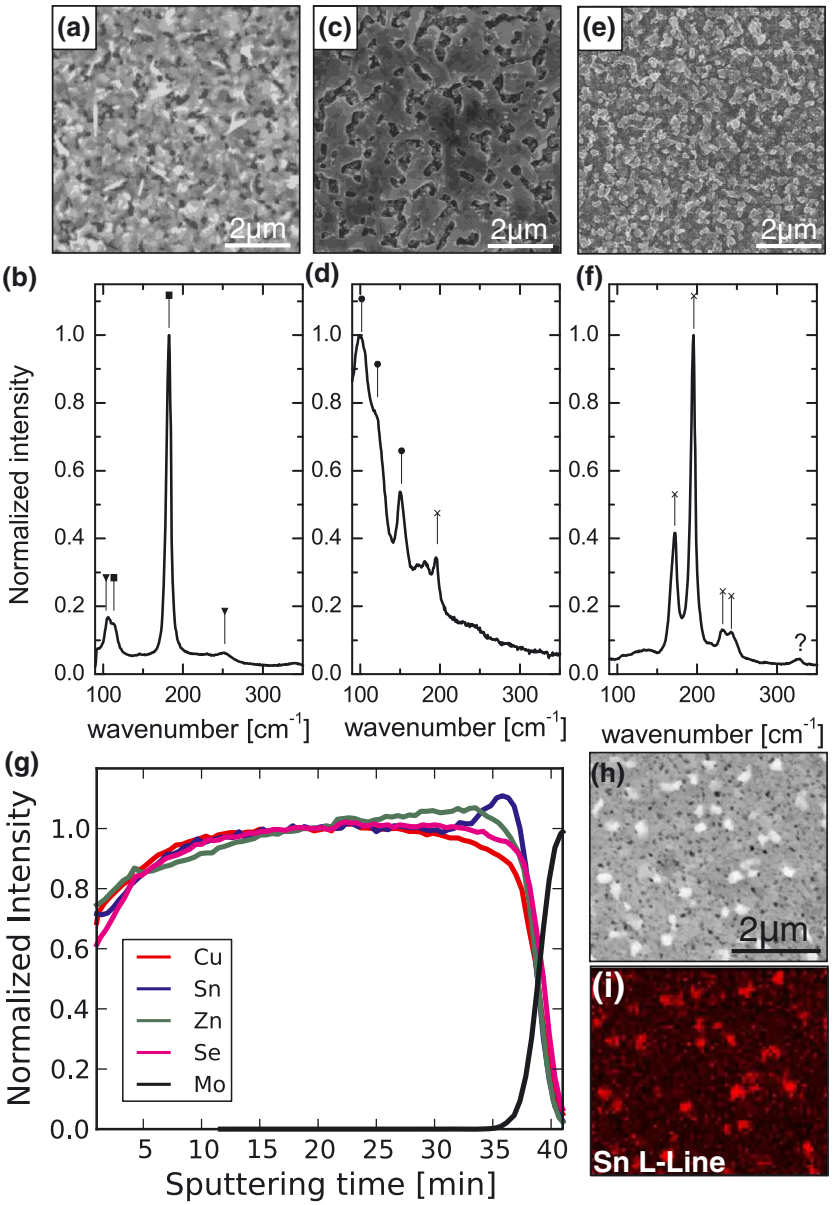

Figure 1. (a–f) Scanning electron microscopy micrographs and corresponding Raman spectra of the absorber, (a,b) prior to the final heat treatment, (c,d) after the heat treatment, and (e,f) after HCl etching. The CZTSe Raman modes are marked with an ×, SnSe modes with •, $SnSe_2$ with ■, and Se with ▼. (g) Secondary ion mass spectrometry analysis of the absorber layer after HCl etching. Intensities have been normalized at 19-min sputtering time, that is, in the middle of the layer. (h) Scanning electron microscopy micrograph of the backside of the layer, and (i) energy dispersive X-ray mapping of the Sn L-line of morphology shown in (h).

perfectly correlated with the white spots. Moreover, the Cu signal is anti-correlated (not shown here). We therefore attribute the secondary phase at the back of the absorber to an $SnSe_x$ phase.

The current–voltage characteristic of the best-performing solar cell is shown in Figure 2 together with the corresponding QE measurements. The solar cell parameters can be found in Table I. A maximum solar cell efficiency of 5.1% has been achieved. An open circuit voltage of 340 mV, which is only 37 mV lower than the current CZTSe record cell produced by NREL Laboratory [2], could be achieved. The series resistance is well below 1 Ωcm^2 in the dark and under illumination, which is already a significant difference compared with most solar cells produced by IBM [13] (except the current record cell by Todorov *et al.* [1]). The comparison between this solar cell and the current CZTSe record cell shows that the largest deficits are the short circuit density (27 mA/cm^2 compared with 37.4 mA/cm^2) and the fill factor (55% compared with 64.9%). The loss in *FF* can be associated

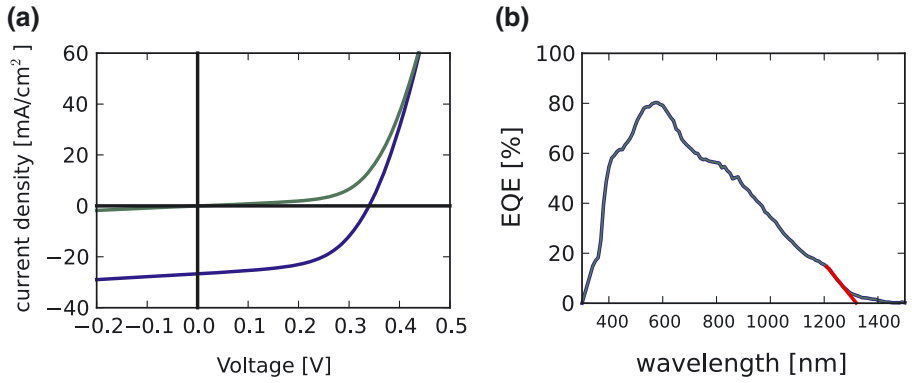

Figure 2. Current–voltage curve of the best CZTSe thin film solar cell produced with a capping layer. (b) Quantum efficiency (QE) measurements of the solar cell presented in (a). The bandgap of the absorber is deduced via linear extrapolation of the low-energy slope of the QE as shown in (b).

Table I. Solar cell parameters of the best-performing CZTSe solar cell presented in Figure 2.

η (%)	FF (%)	V_{OC} (mV)	J_{SC} (mA/cm^2)	R_S (Ωcm^2)	G_{sh}(S/cm^2)	A	j_0 (mA/cm^2)
5.1	55	340	27	0.59	$1.1 \cdot 10^{-2}$	1.76	$2 \cdot 10^{-5}$
Dark				0.62	$8.9 \cdot 10^{-3}$	1.5	$2.5 \cdot 10^{-6}$

The efficiency η, the fill factor FF, the open circuit voltage V_{OC}, the short circuit current density J_{SC}, the series resistance R_S, the shunt conductance G_{sh}, the diode quality factor A, and the saturation current density j_0 are indicated. The values have been deduced with the method introduced by Sites and Mauke [18].

with the rather high j_0 of $2 \cdot 10^{-5}$ A/cm^2 and the high shunt conductance. The QE measurements presented in Figure 2(b) show a very poor response towards high wavelengths. Moreover, we observe a significant decrease at around 750 nm. Currently, we attribute this response to $SnSe_2$ inclusions or remainders at the surface because this material is known to exhibit a bandgap between 1.0 and 1.6 eV [19]. This is a reasonable assumption because we observe a secondary phase containing Sn and Se at the CZTSe/$MoSe_2$ interface. Because the $SnSe_2$ source is on top of the absorber (capping layer), it is likely that we also have traces of $SnSe_2$ present in the bulk of the absorber. However, further measurements have to be made in order to corroborate this explanation.

In Figure 3(a), the temperature dependence of the solar cell efficiency together with the evolution of the short circuit current density is presented. The first observation is that the solar cell efficiency increases linearly with decreasing temperature, which is the usual observation for well-behaved solar cells. It has to be emphasized that this temperature-dependent J–V behavior is different from most other CZTSSe devices described in literature [13]. All other measurements showed a decrease of the solar cell efficiency, which resulted from strong photocurrent suppression, which has been associated with a diverging series resistance at low temperatures. Only recently that an almost S-free 10.1% CZTSSe solar cell [20] showed a much weaker temperature dependence with only a factor of 10 increase in R_S at low temperature. In the present case, there is no change with decreasing temperature as shown in Figure 3(b), where the series resistance is roughly 0.6 Ωcm^2 over the complete temperature range. Moreover, there is no significant difference between the dark and illuminated series resistance R_S. This observation is also different from other CZTSSe thin film solar cells where the dark and illuminated R_S are usually very different [3,21].

The dominant recombination pathway in the solar cell has been investigated via the temperature dependence of the open circuit voltage, which is described by the following equation [22]:

$$V_{OC} = \frac{E_a}{q} - \frac{AkT}{q} \ln \frac{J_{00}}{J_{ph}} \quad (1)$$

The energy E_a describes the activation energy of the saturation current density, A is the diode quality factor, k the Boltzmann constant, T the temperature, J_{00} the prefactor of the saturation current density, and J_{ph} the photocurrent density. From Equation (1), it follows that V_{OC} extrapolates to E_a at $T = 0$. If E_a is equal to the fundamental bandgap E_g of the absorber, then the dominant recombination pathway is situated in the bulk of the absorber. If, however, E_a is smaller than E_g, then the dominated recombination pathway is situated at the interface of the heterojunction. The bandgap in this case is deduced with external quantum efficiency measurements and with PL shown in Figures 2(b) and 3(d). The results are presented in Figure 3(c). The bandgap from the QE measurements, the extrapolation of V_{OC} with temperature, and the PL measurements are identical within the experimental uncertainties ($\approx$ 0.95 eV). We can therefore conclude that the dominant recombination pathway is not situated at the

DOI: 10.1002/pip

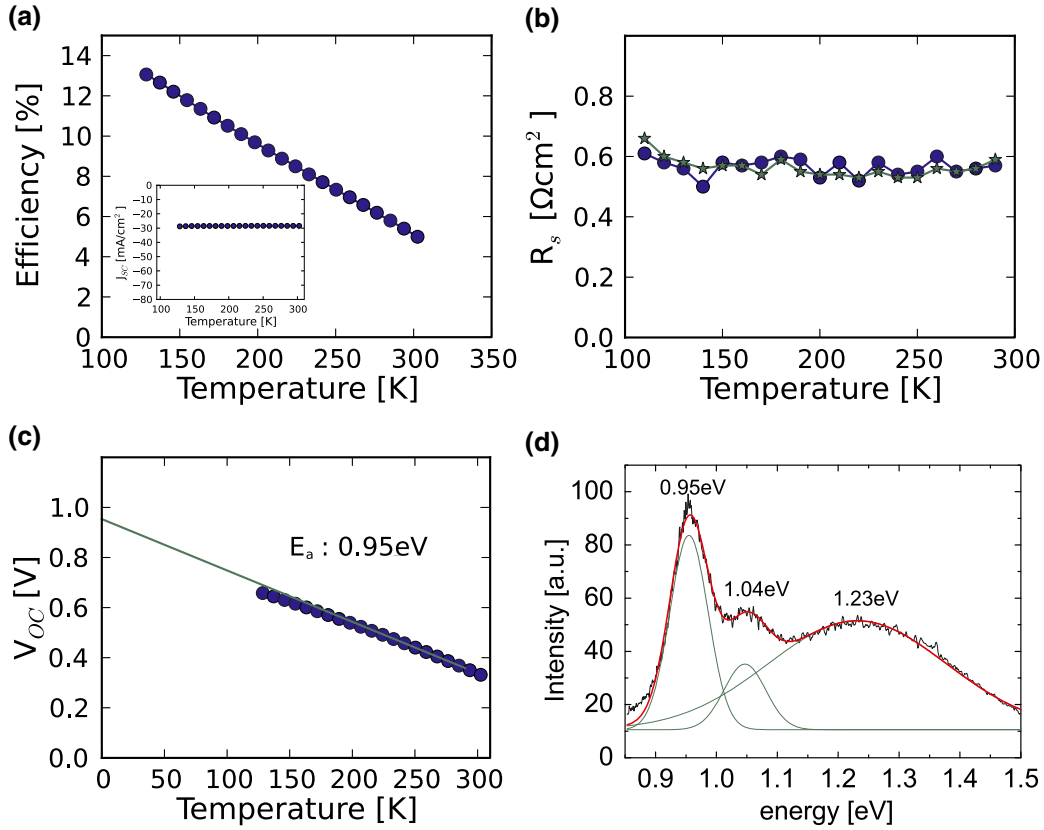

Figure 3. (a) Temperature dependence of the solar cell efficiency and of the short circuit current density, (b) series resistance as a function of temperature (●, dark; ⋆, illuminated), (c) open circuit voltage as a function of temperature (the line corresponds to a linear extrapolation to 0 K), and (d) photoluminescence spectra recorded at room temperature (the individual peak positions and shapes have been extracted via peak deconvolution).

interface of the heterojunction but is situated in the bulk of the absorber. However, the room temperature PL measurements are not easy to interpret because we observe two other band-to-band transitions in the absorber. We already assigned the high bandgap transition at 1.23 eV to a defect transition in doped ZnSe [10]. The 1.04-eV transition is not clear yet. In any case, the multiple peak structure in the room temperature PL is an undesirable property of the absorber because different bandgaps in the absorber inevitably lead to efficiency losses [23].

Finally, temperature dependence of the solar cell parameters have been investigated under different illumination conditions. In Figure 4, the *I–V* curves of the solar cell in the dark, under illumination with white light, and under illumination with wavelengths higher than 590 nm [Figure 4(c)] and higher than 495 nm [Figure 4(d)] are shown. In the 590-nm case, no carriers are generated in the CdS buffer layer (bandgap: 2.5 eV [24]), whereas the 495-nm filter cuts off slightly above the CdS bandgap. In order to reduce effects due to different illumination intensities, the solar cells have been illuminated such that they exhibit the same short circuit current density at room temperature. The dark and illuminated curves do not exhibit any severe distortions from the diode behavior. As already shown in Figure 3, no increase in the series resistance is visible over the complete temperature range. However, if the solar cell is illuminated with red light, the *I–V* curves differ substantially. We observe a strong loss in fill factor towards lower temperatures. This phenomenon, which is known as red-kink effect, is only visible if the light with wavelength smaller than the CdS bandgap is used [25]. If the 495-nm filter is used, the red kink disappears, and the curves resemble the white light-illuminated case. The same effect has been observed in Cu(In,Ga)Se_2 (CIGS) solar cells, and a number of different explanations are available. In any case, a barrier for the photocurrent has to be present, which can be imposed by a band discontinuity, a bandgap gradient, or a specific doping profile (p^+-layer) [22].

Details of the origin of the red-kink effect in CZTSe will not be discussed here. However, the present device exhibits similar characteristics as the closely related CIGS thin film solar cells (low series resistance down to low temperature, dominant bulk recombination). It is likely that the models developed for CIGS can also be used to explain some of the observations presented in this manuscript. However, more

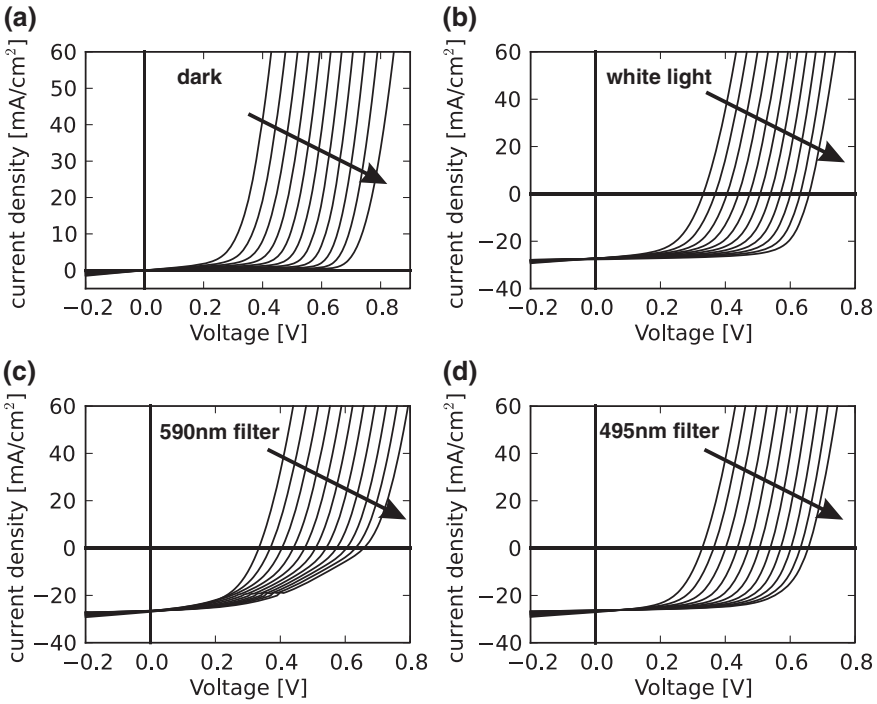

Figure 4. Temperature-dependent current–voltage analysis for different illuminations: (a) dark, (b) white light, (c) light with wavelengths higher than 590 nm, and (d) light with wavelength higher than 495 nm. Arrow points towards lower temperature (T = 120 K–300 K).

experimental data have to be available in order to determine which model explains the observations in the CZTSe thin film solar cells best.

One important point has to be discussed here. Why is there no large increase in series resistance at low temperature? Currently, the series resistance is attributed to a blocking Schottky contact at the Mo–CZTSe interface or, more recently, to a dielectric freeze out at intermediate temperatures [26]. These studies have been limited to mixed sulfur/selenium devices. In this case, the absorber does not contain sulfur. In a recent study [27], we showed that we only observe a large series resistance increase if sulfur is present in the absorber or if the Zn/Sn ratio in the absorber layers is much higher in the near-surface region compared with the bulk composition. In both cases, we attributed the observations to a ZnS(e) secondary phase, which is present in Zn-rich absorber layers at the heterojunction interface. However, the ZnS secondary phase (in the case of mixed S/Se devices) seems to be much more harmful to the performance of the device than the ZnSe secondary phase. This is most likely due to the much higher bandgap of the ZnS compared with ZnSe. In the present case, we do not observe a large increase of the Zn/Sn in the near-surface region. Consequently, we do not observe a strong increase of the series resistance in the J–V curves at low temperatures. For a more detailed discussion of the differences between seleno-sulfide and pure selenide kesterite devices, the reader is referred to reference [27].

4. CONCLUSION

In summary, we demonstrated that the decomposition of CZTSe during the high-temperature treatment can be inhibited with a $SnSe_2$ capping layer. A solar cell efficiency exceeding 5% could be achieved. Moreover, the solar cells do not show a high series resistance anymore, the dominant interface recombination is situated in the bulk of the absorber, and a red kink has been observed if no carriers are generated in the CdS buffer layer. However, an in-depth analysis of possible $SnSe_x$ inclusions in the bulk of the absorbers is necessary in order to further improve the solar cell efficiency.

ACKNOWLEDGEMENTS

The authors acknowledge FNR Luxembourg for funding through the Project No. C08/MS/20, TDK Corporation in the framework of the TDK Europe Professorship, Bosch GmbH for funding, and M. Kurihara at TDK Corporation for solar cell finishing.

REFERENCES

1. Todorov TK, Tang J, Bag S, Gunawan O, Gokmen T, Zhu Y, Mitzi DB. 11% efficiency: characteristics of state-of-the-art $Cu_2ZnSn(S,Se)_4$ solar cells. *Advanced Energy Materials* 2012. DOI: 10.1002/aenm.201200348

2. Repins I, Beall C, Vora N, De Hart C, Kuciauskas D, Dippo P, To B, Mann J, Hsu W-C, Goodrich A, Noufi R. Co-evaporated $Cu_2ZnSnSe_4$ films and devices. *Solar Energy Materials and Solar Cells* 2012; **101**: 154–159.
3. Barkhouse DAR, Gunawan O, Gokmen T, Todorov TK, Mitzi DB. Device characteristics of a 10.1% hydrazine-processed $Cu_2ZnSn(Se,S)_4$ solar cell. *Progress in Photovoltaics: Research and Applications* 2011. DOI: 10.1002/pip.1160
4. Guo Q, Ford GM, Yang WC, Walker BC, Stach EA, Hillhouse HW, Agrawal R. Fabrication of 7.2% efficient CZTSSe solar cells using CZTS nanocrystals. *Journal of the American Chemical Society* 2010; **132**: 17384–17386.
5. Katagiri H, Jimbo K, Yamada S, Kamimura T, Maw WS, Fukano T, Ito T, Motohiro T. Enhanced conversion efficiencies of Cu_2ZnSnS_4-based thin film solar cells by using preferential etching technique. *Applied Physics Express* 2008; **1**: 041201-1–041201-2.
6. Todorov TK, Reuter KB, Mitzi DB. High-efficiency solar cell with Earth-abundant liquid-processed absorber. *Advanced Materials* 2010; **22**: 1–4.
7. Wang K, Gunawan O, Todorov T, Shin B, Chey SJ, Bojarczuk NA, Mitzi D, Guha S. Thermally evaporated Cu_2ZnSnS_4 solar cells. *Applied Physics Letters* 2010; **97**: 143508-1–143508-3.
8. Redinger A, Berg DM, Dale PJ, Siebentritt S. The consequences of kesterite equilibria for efficient solar cells. *Journal of the American Chemical Society* 2011; **133**: 3320–3323.
9. Redinger A, Siebentritt S. Coevaporation of $Cu_2ZnSnSe_4$ thin films. *Applied Physics Letters* 2010; **97**: 092111-1–092111-3.
10. Redinger A, Berg DM, Dale PJ, Djemour R, Gütay L, Eisenbarth T, Valle N, Siebentritt S. Route toward high-efficiency single-phase $Cu_2ZnSn(S,Se)_4$ thin-film solar cells: model experiments and literature review. *IEEE, Journal for Photovoltaics* 2011; **1**: 200–206.
11. Scragg JJ, Ericson T, Izquierdo-Roca V, Fontané X, Pérez-Rodríguez A, Kubart T, Edoff M, Platzer-Björkman C. Rapid annealing of reactively sputtered precursors for Cu_2ZnSnS_4 solar cells. *Progress in Photovoltaics: Research and Applications* 2012. DOI: 10.1002/pip.2265
12. Patent filed on 26.04.2012 in Luxembourg, Nr. 91986.
13. Mitzi D, Gunawan O, Todorov T, Wang K, Supratik G. The path towards a high-performance solution-processed kesterite solar cell. *Solar Energy Materials and Solar Cells* 2011; **95**: 1421–1436.
14. Mead DG, Irwin JC. Raman spectra of SnS_2 and $SnSe_2$. *Solid State Communications* 1976; **20**: 885–887.
15. Lucovsky G, Mooradian A, Taylor W, Wright GB, Keezer RC. Identification of the fundamental vibrational modes of trigonal, α-monoclinic and amorphous selenium. *Solid State Communications* 1967; **5**: 113–117.
16. Soliman HS, Abdel Hady DA, Abdel Rahman KF, Youssef SB, El-Shazly AA. Optical properties of tin-selenid films. *Physica A* 1995; **216**: 77–84.
17. Redinger A, Hönes K, Fontané X, Izquierdo-Roca V, Saucedo E, Valle N, Pérez-Rodríguez A, Siebentritt S. Detection of a ZnSe secondary phase in coevaporated $Cu_2ZnSnSe_4$ thin films. *Applied Physics Letters* 2011; **98**: 101907-1–101907-3.
18. Sites JR, Mauk PH. Diode quality factor determination for thin-film solar cells. *Solar Cells* 1989; **27**: 411–417.
19. Domingo G, Itoga RS, Kannewurf CR. Fundamental optical absorption in SnS_2 and $SnSe_2$. *Physical Review* 1966; **143**: 536–541.
20. Bag S, Gunawan O, Gokmen T, Zhu Y, Todorov TK, Mitzi DB. Low bandgap liquid-processed CZTSe solar cell with 10.1% efficiency. *Energy & Environmental Science* 2012; **5**: 7060–7065.
21. Shin B, Gunawan O, Zhu Y, Bojarczuk NA, Chey SJ, Guha S. Thin film solar cell with 8.4% power conversion efficiency using an Earth-abundant Cu_2ZnSnS_4 absorber. *Progress in Photovoltaics: Research and Applications* 2011. DOI: 10.1002/pip.1174
22. Scheer R, Schock HW. *Chalcogenide Photovoltaics*. Wiley-VCH Verlag GmbH and Co. KGaA: Weinheim, 2011.
23. Rau U, Werner JH. Radiative efficiency limits of solar cells with lateral band-gap fluctuations. *Applied Physics Letters* 2004; **84**: 3735–3737.
24. Sze SM, Ng KK. *Physics of Semiconductor Devices*. John Wiley and Sons, Inc.: Hoboken, New Jersey, 2006.
25. Eisgruber IL, Granata JE, Sites JR, Hou J, Kessler J. Blue-photon modification of nonstandard diode barrier in $CuInSe_2$ solar cells. *Solar Energy Materials and Solar Cells* 1998; **53**: 367–377.
26. Gunawan O, Gokmen T, Warren CW, Cohen JD, Todorov TK, Barkhouse DA, Bag S, Tang J, Shin B, Mitzi DB. Electronic properties of the $Cu_2ZnSn(Se,S)_4$ absorber layer in solar cells as revealed by admittance spectroscopy and related methods. *Applied Physics Letters* 2012; **100**: 253905-1–253905-4.
27. Redinger A, Mousel M, Wolter MH, Valle N, Siebentritt S. *Thin Solid Films* 2012, DOI: 10.1016/j.tsf.2012.11.111.